Received: 29 March 2022 | Revised: 7 October 2022 | Accepted: 11 October 2022

DOI: 10.1002/asl.1141

RESEARCH ARTICLE

Atmospheric Science Letters RMetS

Intensification of a distant hurricane by warm-core eddies in the Gulf Stream in boreal fall

Keita Fujiwara[1] | **Ryuichi Kawamura**[2]

[1]Disaster Prevention Research Institute, Kyoto University, Kyoto, Japan

[2]Department of Earth and Planetary Sciences, Kyushu University, Fukuoka, Japan

Correspondence
Keita Fujiwara, Disaster Prevention Research Institute, Kyoto University Gokasho, Uji, Kyoto 611-0011, Japan.
Email: keita.fujiwara926@gmail.com

Funding information
Japan Society for the Promotion of Science, Grant/Award Numbers: JP19H05696, JP20H00289, JP20J11837

Abstract

This study investigated how warm-core eddies (WCEs) in the Gulf Stream (GS) modulated the intensity of a distant tropical cyclone (TC) approaching the current in October. We performed cloud-resolving regional simulations including a control run with the observed WCEs and a sensitivity run excluding the WCEs. These simulations found that the WCEs played a favorable role in the development of the distant TC. The WCEs affected the synoptic-scale thermodynamic environments over the North Atlantic through the enhanced heat and moisture supply from the GS, increasing the moisture imports toward the distant TC. The WCEs-enhanced moisture influx created very moist environments in the inner core. This inner-core moistening was favorable for deep eyewall convection and an associated TC secondary circulation, leading to TC development. This result indicates the importance of WCEs in facilitating the remote process leading to TC development that previous studies have proposed.

KEYWORDS

the Gulf Stream, tropical cyclone, warm-core eddies

1 | INTRODUCTION

The non-homogeneous ocean structures related with mesoscale ocean eddies have a significant impact on tropical cyclone (TC) intensity (e.g., Liang et al., 2018; Lin et al., 2005, 2008; Ma, 2020). Mesoscale warm ocean eddies, referred to as warm-core eddies (WCEs), is particularly important in TC intensification (Hong et al., 2000; Shay, 2010). A statistical research has reported that the regions where intense TCs are observed correspond to those of active WCEs, and 70% of observed TCs over the Western North Pacific encounter the WCEs at least one time (Ma et al., 2017). Under these backgrounds, a lot of studies regarding the local influence of ocean conditions associated with the WCEs on TC intensity have been conducted for the real TCs such as Hurricane Opal (Shay et al., 2000), Hurricane Katrina (Wu et al., 2007), and Typhoon Soudelor (Li & Huang, 2019) and for the idealized TC (Sun et al., 2020).

On the other hand, several recent studies have pointed out the significant role of remote ocean environments in TC strength (Fujiwara et al., 2017, 2020a, 2020b; Hegde et al., 2016). Fujiwara and Kawamura (2021, hereafter FK21) revealed the modulations of TC intensity and structure through the remote impact of large-scale SST changes over the Kuroshio in boreal fall. Some of northward-traveling TCs over the Philippine Sea encountered an eastward-moving anticyclone around Japan in

boreal fall, inducing dry and cold northeasterly winds in the lower troposphere over the Kuroshio. According to FK21, the warm (cold) SST anomalies over the entire Kuroshio enhanced (restrained) the surface evaporation from the current under the dominance of the low-level northeasterlies and increased (decreased) the transports of high-enthalpy air toward the distant TCs, affecting the thermodynamic and dynamic processes in the inner core.

It is well known that the WCEs are very pronounced in the western boundary currents (WBCs; e.g., Ducet et al., 2000; Renault et al., 2017). The active WCEs around the WBCs have a significant local impact on the activity of landfalling TCs when they pass the currents (Jaimes et al., 2011). In addition to such a local impact, we also have a hypothesis that SST changes associated with the active WCEs in the WBCs remotely affect TC intensity. FK21 has not fully investigated whether the local SST structures associated with the WCEs in the WBCs modulate TC development over the remote ocean or not. Furthermore, it remains uncertain whether the remote process examined in FK21 can also apply to TCs around the Gulf Stream (GS), which is a strong WBC in the midlatitudes of the Northern Hemisphere.

The main purpose of this study is to explore how the WCEs in the GS modulate the remote process leading to TC development that FK21 have proposed. Around the GS in fall, low-level northeasterly winds tend to prevail concurrent with the development of synoptic-scale highs over the North American continent due to land-surface cooling (Figure S1). Since the northeasterly flows from the continent in fall are cold and dry, surface evaporation from the underlying GS is significantly enhanced, suggesting that the abundant moisture evaporated from the GS is more easily imported into the distant TC approaching the current in fall than in summer. Thus, we specifically focus on hurricane approaching the GS in a fall season. This study addresses the question mentioned above, using numerical simulations regarding hurricane and WCEs aided by Lagrangian diagnostics.

2 | A CASE OVERVIEW AND MODEL SETUP

2.1 | A case overview

To explore our hypothesis, we focused on Hurricane Nicole approaching the GS in October 2016. Figure 1 shows the observed synoptic-scale environments during the development and mature phases of Nicole. When Nicole moved northward, strong northerly or northeasterly winds prevailed around the GS due to the combination of an anticyclone over the North American continent and Nicole (Figure 1a–c). Satellite observation (J-OFURO3; Tomita et al., 2019, 2021) captured the active heat and vapor supply from the GS although J-OFURO3 cannot accurately estimate the fluxes in the TC inner core due to issues with the construction method (Wada et al., 2020). These synoptic-scale atmospheric and ocean environments were similar to those in FK21.

Another very important point is that local warm SST anomalies in excess of +2°C (Figure 1d–f) are well consistent with the areas of anticyclonic geostrophic currents and positive sea level anomalies (symbols A–C in Figure 1g–i), indicating that WCEs predominated in the GS when Nicole was approaching the current. The WCEs created the local maximum of active heat and vapor supply from the GS, inferring that the WCEs in the GS may remotely modulate Nicole's development through the remote process discussed by FK21.

2.2 | Model description and simulation design

The numerical simulations for Hurricane Nicole were performed using the Cloud Resolving Storm Simulator (CReSS; Tsuboki & Sakakibara, 2002) without atmosphere–ocean interaction. The parameterization of the rain process was based on Murakami (1990), Ikawa and Saito (1991), and Murakami et al. (1994). The subgrid-scaled turbulent mixing process was derived from the method of Deardorff (1980). The method of Kondo (1975) and Louis et al. (1981) were used in the surface momentum and heat flux over the ocean and land, respectively. The method of Tsuboki and Sakakibara (2002) was applied to the shortwave and longwave radiation processes. The simulated domain covered the North Atlantic sectors (15° N–57° N and 37° W–85° W) with a horizontal resolution of 0.04° and 57 vertical layers. The simulated period was during the 108 h from 1200 UTC on 9 October 2016 to 0000 UTC on 14 October 2016. The initial and boundary conditions were obtained from the 6-hourly and 0.25°-gridded Global Forecast System (GFS) data provided by the National Centers for Environmental Prediction (NCEP) (NCEP, 2015). The SST data was obtained from the daily and 0.25°-gridded Optimum Interpolation Sea Surface Temperature (OISST) V2.1 (Huang et al., 2021). This numerical simulation was referred to as a control (CTL) run. The sea surface condition in the CTL run was time-fixed SST at the initial time.

To investigate the impact of WCEs in the GS on the intensity of Hurricane Nicole, we conducted a sensitivity experiment that the SSTs within the domain enclosed by blue lines in Figure 2a were replaced by climate values. The climate SSTs were the daily mean values on 9 October averaged over the period of 1981–2020. In the

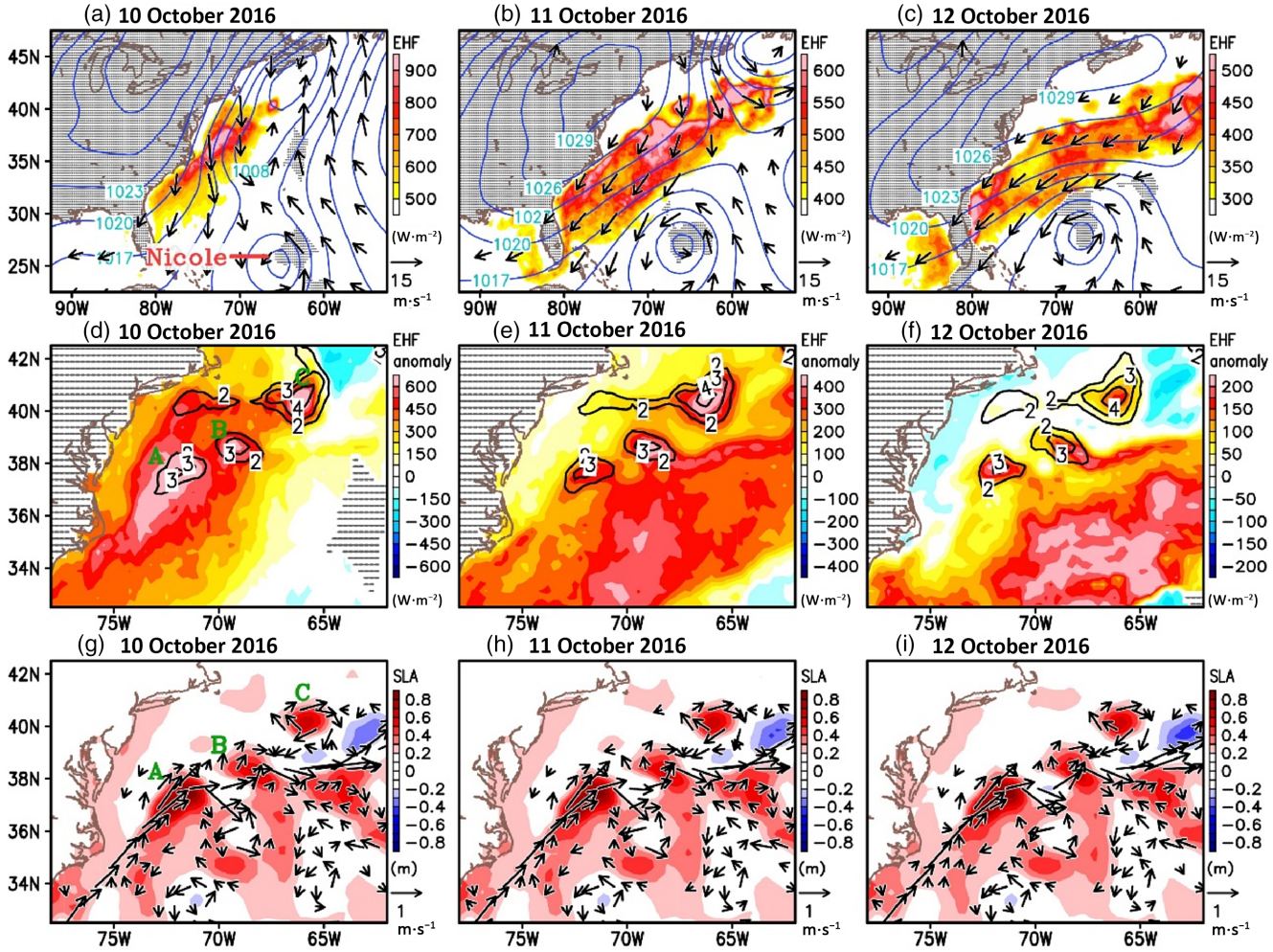

FIGURE 1 (a–c) Horizontal distributions of the daily-mean surface enthalpy heat flux (EHF; shading), the sea level pressure (SLP; blue contours with 3 hPa intervals), and the 10 m wind (vectors) on (a) 10, (b) 11, and (c) 12 October 2016. The EHF is the sum of latent heat flux (LHF) and sensible heat flux (SHF). Positive values in EHF are for sea-to-air moisture and heat supply. Gray dotted areas show the missing value of EHF. Vectors of <5 $m \cdot s^{-1}$ are not shown. The LHF, SHF, SST, and 10 m wind are derived from the satellite-based observation (J-OFURO3; Tomita et al., 2019, 2021). The SLP is obtained from the Japanese 55-year reanalysis dataset (JRA-55; Kobayashi et al., 2015). (d–f) Same as in (a–c), but for the magnified views of EHF anomaly (shading) and SST anomaly (contours with 1°C intervals). Contours of 0°C and ±1°C SST anomalies are not shown. The EHF and SST anomalies are deviation with respect to a 30-year mean period (1988–2017). (g–i) Same as in (d–f), but for the sea level anomaly (SLA; shading) and absolute geostrophic velocity (vectors) derived from Data Unification and Altimeter Combination System (DUACS; Taburet et al., 2019). The SLA is calculated with respect to a 20-year mean reference period (1993–2012). Vectors of <0.25 $m \cdot s^{-1}$ are not shown. The symbols (A–C) denote the locations of warm core eddies (WCEs) mentioned in this study.

sensitivity run, the WCEs in the GS were perfectly excluded (see shaded in Figure 2a). We referred to the sensitivity experiment as a climate (CLM) run. Since the WCEs are primarily responsible for the warm SST anomalies in the modified domain, the removal of WCEs decreased an area-mean SST by 2.24°C in the modified SST area. We also conducted an additional experiment in which inhomogenous SST structures in the modified domain are emphasized; the SSTs in the domain were uniformly modified by warming 2.24°C relative to the climate SSTs. The second sensitivity experiment was referred to as a CLM-plus run. The area-mean SST value in the modified region in the CLM-plus run was the same as that in the CTL run, but fine ocean structures in the GS were different between the two runs (see shaded in Figure 2c).

3 | RESULTS

Figure 2 shows the track and central pressure (CP) in the best track analysis (HURDAT2; Landsea & Franklin, 2013) and simulations. The observed Nicole traveled northward over the ocean more than 800 km

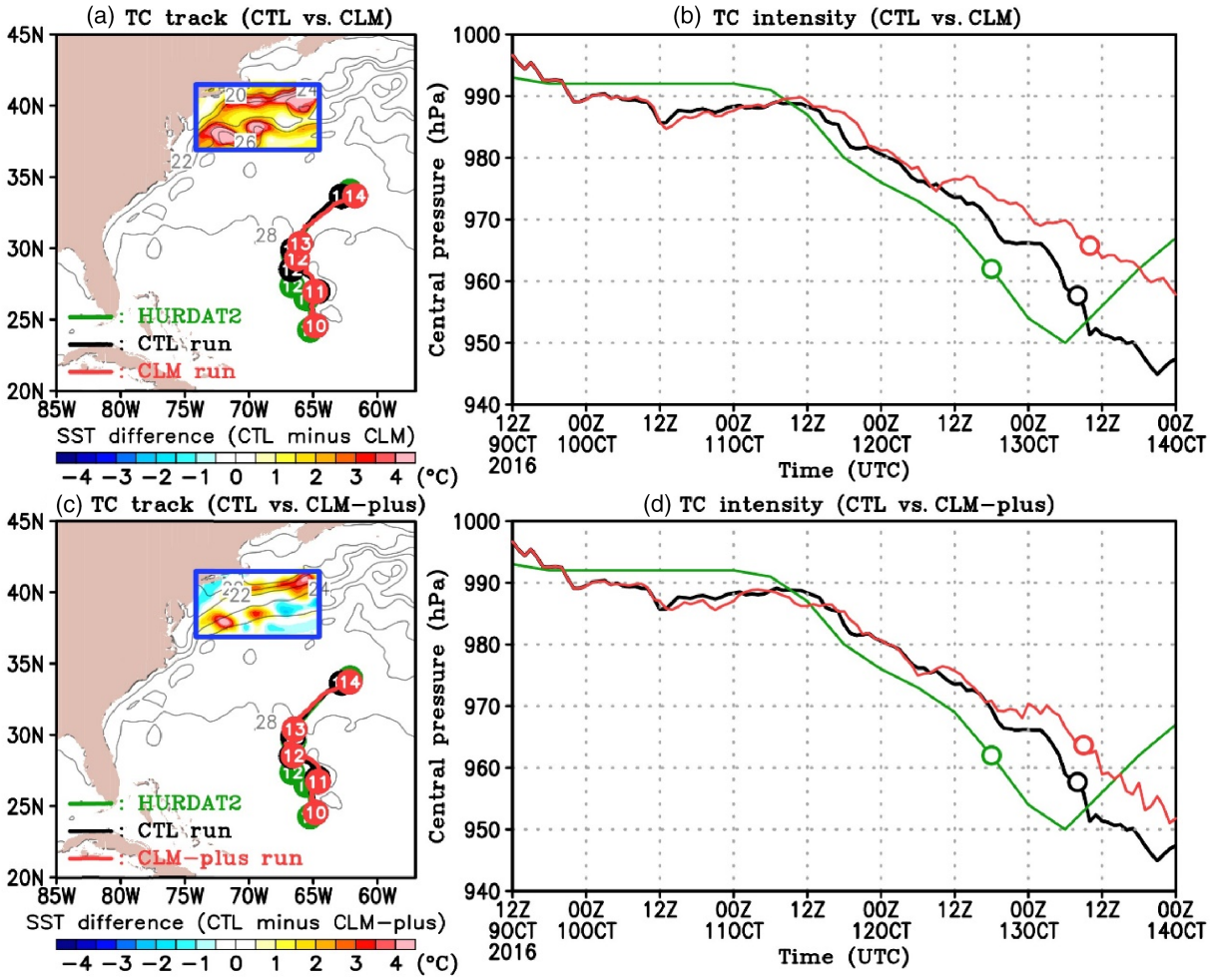

FIGURE 2 (a) TC tracks in the HURDAT2 (green line), CTL run (black line), and CLM run (red line). The circle symbols indicate TC locations at 0000 UTC on each day. The horizontal distributions of the time-fixed SST (contours with 2°C intervals) and its difference between the CTL and CLM runs (shading). (b) Time evolution of the central pressure in the HURDAT2 (green line), CTL run (black line), and CLM run (red line). The circle symbols denote the time of the maximum deepening rate. (c,d) Same as in (a) and (b), but for the results of CTL and CLM-plus runs.

away from the WCEs, and its CP started to decrease after 0600 UTC on 11 October. The maximum deepening rate, 12-hourly change in CP, was observed at 1800 UTC on 12 October. In the CTL run, the track successfully followed the observation during the development and mature stages on 12–13 October. The CP time series was well reproduced, although the time of the maximum deepening rate had a delay of 14 h. These comparisons indicated that the CTL run generally captured the basic features of the observation. In the CLM run, the track fairly resembled that in the CTL run during the development and mature stages. As for intensity, a CP difference between the two runs was very small during the days of 9–11 October. The temporal averaged value of CP before the beginning of TC development at 1200 UTC on 11 October was 989.5 (989.4) hPa in the CTL (CLM) run. After approximately 1200 UTC on 12 October, however, the TC development in the CLM run was obviously suppressed as compared with the CTL run. The CP difference between the two runs reached a maximum of 16 hPa. The maximum deepening rate in the CLM run was simulated at 1000 UTC on 13 October, which was almost the same time as in the CTL run. It is noteworthy that during the days of 12–13 October, the CLM-simulated Hurricane Nicole was located about 1000 km away from the modified SST regions. Furthermore, there was little difference in the SST around TC center between the CTL and CLM runs during the period (not shown). A comparison of the CTL and CLM-plus runs showed that the presence of WCEs facilitated the TC development despite that the area-mean SST in the GS was the same between the two runs (Figure 2d). We also obtained similar results in the other experiments forced by the SST conditions changed daily, although the TC intensity

especially in the development phase was somewhat different from that in Figure 2b,d (Figure S2). These results strongly suggest that the WCEs in the GS had the potential to influence the intensity of TC being far away from the WCEs. We, hereafter, focus specifically on the comparisons between the CTL and CLM runs because the difference in TC intensity between the two runs is the most apparent, as indicated in Figure 2b.

We next show the horizontal maps of the SST, surface latent heat flux (LHF), and surface sensible heat flux (SHF) in the CTL and CLM runs (Figure 3). The LHF and SHF were temporally averaged during the simulation period (108 hours). In the CTL run, the LHF and SHF dominated over the WCEs in the GS (Figure 3a,d). The CTL-simulated LHF and SHF were reasonable, although they were somewhat overestimated as compared with those observed (Figure S3). A comparison of the LHF and SHF between the CTL and CLM runs showed that their significant differences appeared just over the large SST difference areas (Figure 3c,f). The LHF (SHF) difference exceeded 200 (60) $W \cdot m^{-2}$ in the region where the SST was 3 K cooler in the CLM run than in the CTL run. We also show the time series of the areal-mean LHF, areal-mean SHF, and areal-mean thermodynamic environments in the planetary boundary layer (PBL) within the oceanic region where the SST was modified (Figure 3g–i). The CLM run decreased both the LHF and SHF over the GS by about 20% as compared with the CTL run (Figure 3g). In accordance with the decreased LHF and SHF, the water vapor mixing ratio (Qv) and equivalent potential temperature (θ_e) over the GS at a 500 m height were ~1 $g \cdot kg^{-1}$ and ~4 K lower in the CLM run than in the CTL run, respectively (Figure 3h,i). The difference in each areal-mean variable between the CTL and CLM runs is statically significant at a 95% confidence level using Student's *t*-test. These differences indicate that the CLM run excluding WCEs created relatively dry and cool PBL conditions over the GS due to the reduced LHF and SHF from the WCEs. We also confirmed that there are no significant differences in upper-tropospheric circulations over the GS between the two runs (not shown).

FK21 reported that relatively moist or dry PBL regions over the KC in response to changes in the LHF and SHF from the current expanded from the KC into a distant TC due to environmental winds. It is, thus, inferred that the WCEs in the GS influenced the PBL

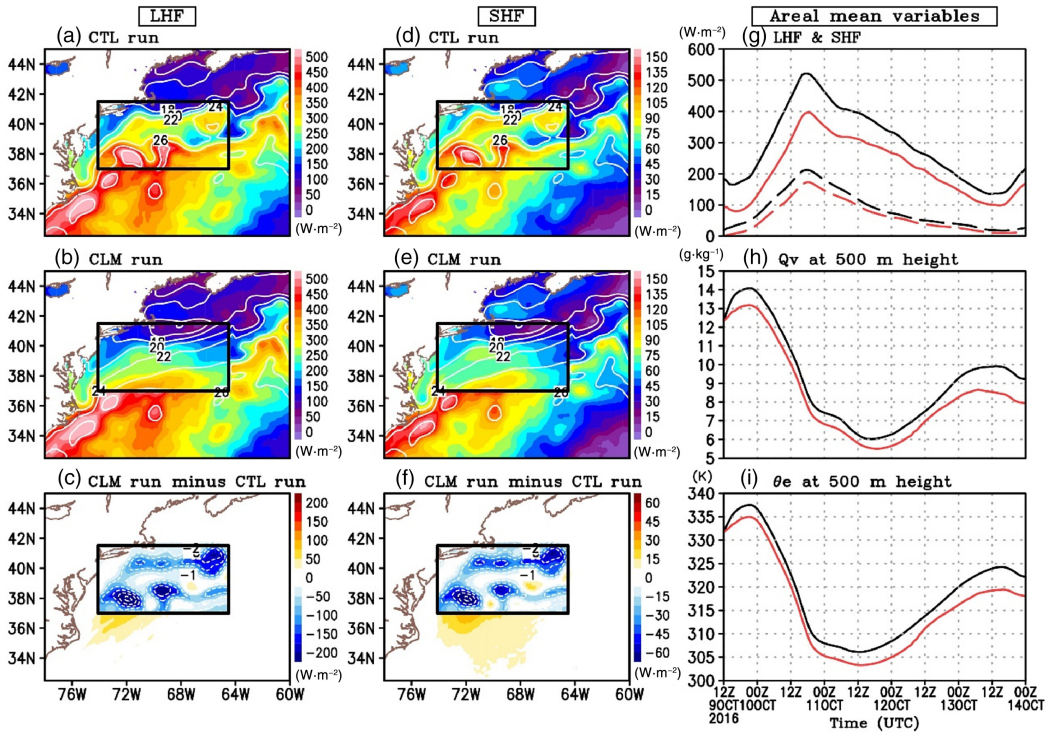

FIGURE 3 (a–c) Horizontal distributions of LHF averaged during the simulation period in (a) the CTL and (b) the CLM runs with time-fixed SST. Contours with 2°C intervals denote the SST distributions. The domain where the SST is modified is enclosed by black lines. (c) Horizontal maps of the differences in the LHF (shading) and SST (contours with 1°C intervals) between the two runs (the CLM run minus the CTL run). Contours of the 0°C SST difference are not shown. (d–f) Same as in (a–c), but for the SHF. (g–i) Areal-mean time series of (g) the LHF (solid line) and SHF (dotted line), (h) the 500 m water vapor mixing ratio (Qv), and (i) the 500 m equivalent potential temperature (θ_e) within a box in (a–f). A black (red) line denotes the results in the CTL (CLM) run.

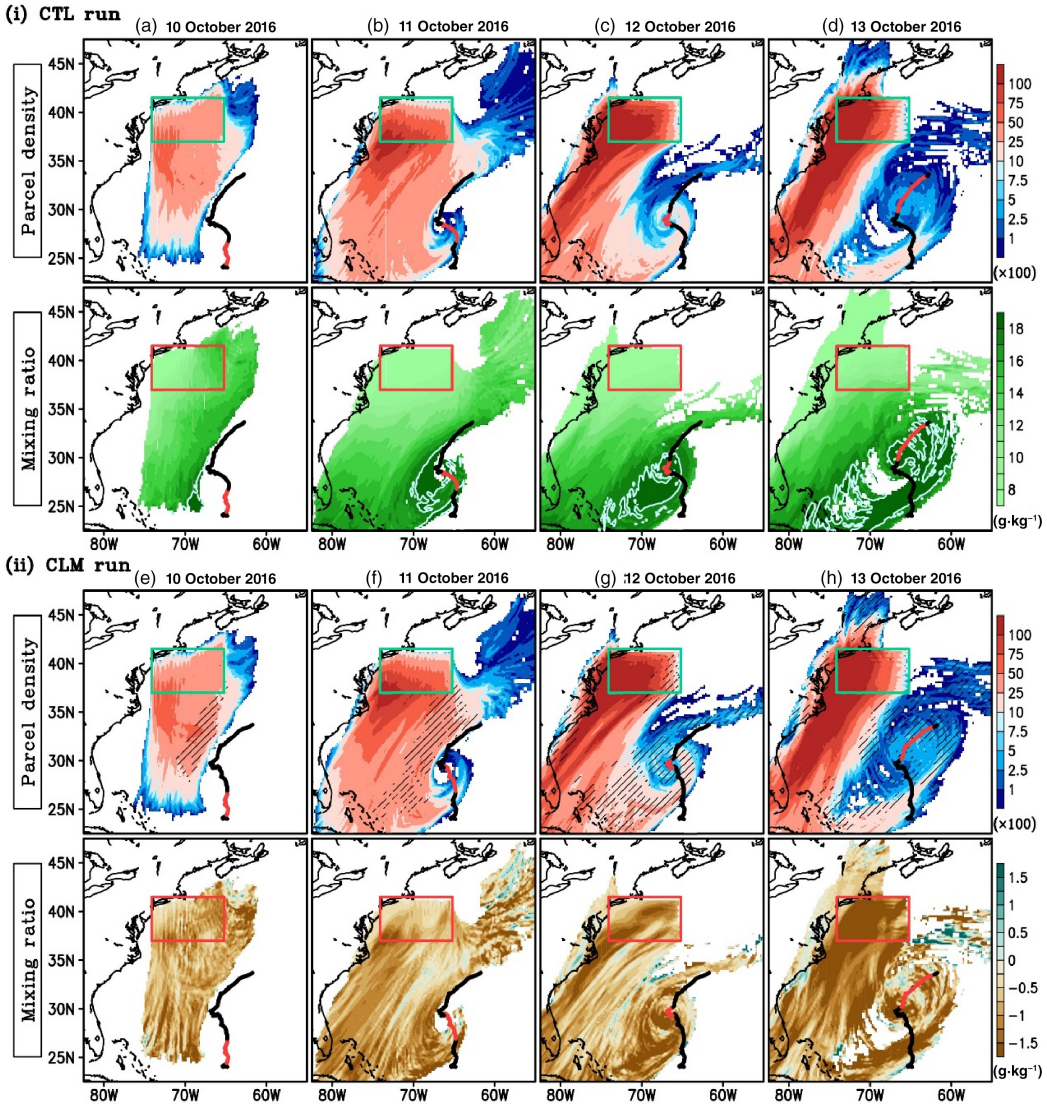

FIGURE 4 (a–d) Maps of the daily accumulated air-parcel density (upper panel) and the daily mean Qv (lower panel) in the PBL on (a) 10, (b) 11, (c) 12, and (d) 13 October 2016, derived from the forward-trajectory analysis in the CTL run. See text for details. A green or red rectangle denotes the domain where the SST was modified. A light blue contour in the lower panel denotes the region where the PBL Qv exceeds 18 g·kg^{-1}. The TC track during the whole simulation period (on each day) is indicated by a black (red) line. (e–h) Same as in (a–d), but for the results of the CLM run. Black hatches denote the difference in the parcel density between the CTL and CLM runs with a 5% level of statistical significance using Student's *t*-test. Note that the Qv in the CLM run is depicted as the difference relative to that in the CTL run.

environments not only around the GS but also in the vicinity of distant Nicole, resulting in modulation of the TC development. To confirm whether the WCEs in the GS actually affected the synoptic-scale PBL conditions, we conducted a forward-trajectory analysis using Lagrangian diagnostics. In the trajectory analysis, we put 375 air parcels at a 500 m height over the modified SST region. The air parcels were released continuously every hour during the period from 1200 UTC on 9 October to 2300 UTC on 13 October. All of them were traced until 0000 UTC on 14 October.

Figure 4 shows the horizontal distributions of the daily accumulated air-parcel density and daily mean Qv in the PBL at a height of <1 km, derived from the trajectory analysis. In the CTL run, air parcels over the GS initially migrated southward along the background northerly winds (see Figure 1). On 11 October, some of the parcels started to move toward the northward-moving TC (Figure 4b). After 12 October, we can clearly see a lot of parcels located near the TC track (Figure 4c,d). In addition, the region where the PBL Qv exceeded 18 g·kg^{-1} surrounded the TC path on 12 and 13 October. In the CLM run, on the other hand, the air parcel behaviors resembled those in the CTL run. The areas with a 5% level of statistical significance using Student's *t*-test on the difference in parcel density between the two runs

appeared only near the TC track. This feature indicated that there was little difference in environmental winds affecting the transport of air parcels from the GS into the vicinity of TC between the two runs. A comparison of the PBL Qv between the two runs clearly showed that relatively dry PBL environments over the GS in the CLM run extended to the vicinity of the distant TC. Especially on 12 and 13 October, corresponding to the development and mature stages, the PBL Qv difference near the TC track between the two runs exceeded 1.5 $g \cdot kg^{-1}$ (Figure 4g,h). Furthermore, the synoptic-scale potential temperature in the PBL tended to be lower in the CLM run than in the CTL run due to the SHF changes in the GS (Figure S4). Since a large SHF over the warm current creates a moist PBL environment through an increase in saturated Qv (FK21), it suggests that the PBL warming due to the WCEs also contributed to the Qv increase in the CTL run. These results reveal that WCEs in the GS enhance the moisture influx toward the distant TC.

To examine the impact of the moisture influx changes associated with WCEs in the GS on the PBL environment of the TC, we next show magnified views of the 6-hourly accumulated parcel density, 6-hourly mean Qv, and 6-hourly mean θ_e within the PBL around the inner core during the period of 0800–1400 (1000–1600) UTC on 13 October in the CTL (CLM) run, when the CP in each run decreased most rapidly (Figure 5). In this study, the inner-core size was simply defined as the region within a radius of 200 km from the TC center. In both the CTL and CLM runs, a lot of air parcels of GS origin were located in the inner core during the development stage (Figure 5a,d). In the CTL run, the parcels contributed to the establishment of a very moist PBL environment with a Qv of more than 19 $g \cdot kg^{-1}$ and a θ_e of more than 360 K in the inner core (Figure 5b,c). In contrast, the inner core in the CLM run was characterized by a lower Qv and θ_e (Figure 5e,f), which is consistent with Figure 4. The areal-mean Qv and θ_e values within the inner core are 18.3 (17.2) $g \cdot kg^{-1}$ and 357.2 (354.3) K in the CTL (CLM) run, respectively. These PBL Qv and θ_e differences between the CTL and CLM runs within the inner core in response to the removal of WCEs in the GS were consistent with the results of FK21.

Figure 5g,h show the radius–height inner-core structures of the azimuthal-mean latent heating (LH), inward moisture flux, and TC secondary circulation during the same period as in Figure 5a–c,d–f, respectively. In the CTL run, as inferred from Figure 4b–d, a significant inward moisture transport reached the eyewall region around a radius of 20–50 km via the PBL during the development stage. In response to the active vapor supply, intense LH in excess of 30 $K \cdot h^{-1}$ occurred within the eyewall, leading to well-organized secondary circulation. In contrast, in the CLM run, the moisture influx in the PBL decreased obviously as compared with the CTL run. The weakening of the moisture influx in the inner core appeared after approximately 1200 UTC on 11 October, concurrent with the beginning of the CP difference (Figure S5a). The time when the PBL moisture influx weakened in the CLM run was also consistent with the timing of the intrusion of air parcels of GS origin into the inner core (Figure S5b). Due to the decrease in moisture influx in association with the removal of WCEs, the eyewall convection and secondary circulation were much weaker in the CLM run than in the CTL run (Figure 5h). In accordance with these differences, an inward momentum advection in the PBL and an upward momentum transport within the eyewall were also fairly reduced in the CLM run (Figure S6), leading to the suppression of a vortex spin-up in the inner core. We also confirmed that vertical wind shear within the inner core between 200 and 850 hPa during the same period as in Figure 5 in the CLM run (19 $m \cdot s^{-1}$) was almost same with that in the CTL run (20 $m \cdot s^{-1}$). These results show that WCEs in the GS affected the development of a distant TC by regulating the moisture influx into the inner core.

4 | SUMMARY

To inspect the impact of warm-core eddies (WCEs) in the Gulf Stream (GS) on the development of Hurricane Nicole approaching the current in October 2016, we conducted a control (CTL) run with an observed sea surface temperature (SST) and a climate (CLM) run with a climate SST in the GS. The CTL run successfully reproduced the active surface evaporation from the WCEs, the tropical cyclone (TC) track, and its intensity change, as compared with the satellite observation and best track dataset. Comparisons between the CTL and CLM runs revealed that the WCEs in the GS played an influential role in facilitating the development of the distant TC. The WCEs modulated the synoptic-scale thermodynamic environment through the increase in heat and moisture supply from the current, leading to abundant moisture transports from the GS into the distant TC. The WCE-enhanced moisture influx created a very moist inner-core environment characterized by high-entropy air in the PBL. The inner-core moistening was favorable for well-organized eyewall convection and associated secondary circulation, leading to TC development. This result reveals that WCEs in the GS affect the remote process leading to hurricane development through the change in moisture influx from the GS. A similar remote process due to the WCEs in the GS is also confirmed by additional simulations for Hurricane Humberto approaching the GS in September 2019,

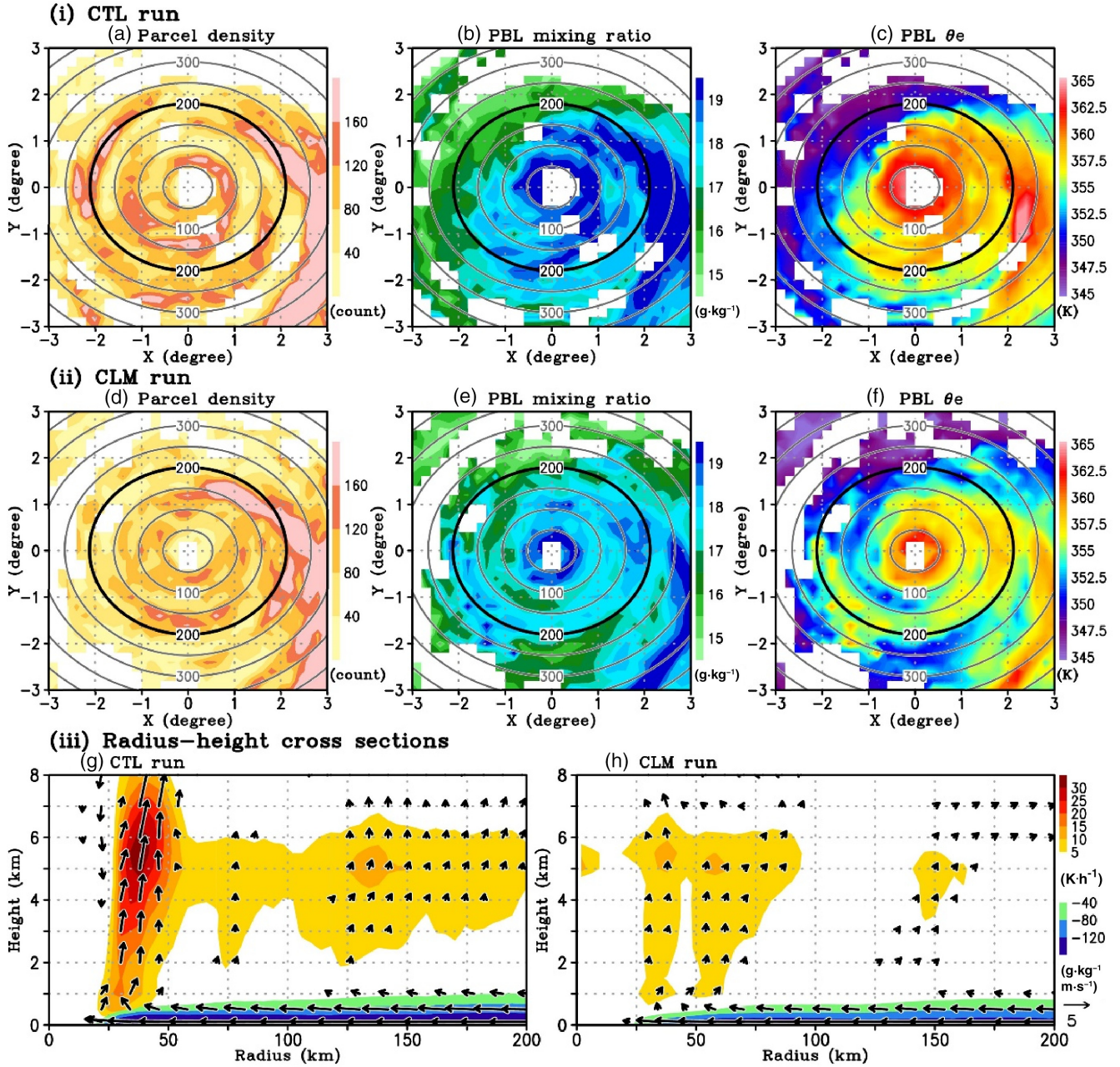

FIGURE 5 (a–c) Horizontal maps of (a) the 6-hourly accumulated parcel density, (b) the 6-hourly mean PBL Qv, and (c) the 6-hourly mean PBL θ_e during the development stage, derived from the forward-trajectory analysis in the CTL run. Gray contours denote the radial distances from the TC center with an interval of 50 km. A black contour of 200 km indicates the inner-core region. (d–f) Same as in (a–c), but for the results of the CLM run. (g) Radius–height cross sections of the azimuthal-mean LH (orange-red shading), the inward moisture flux (green–purple shading), and the TC secondary circulation (vectors) in the CTL run. Each variable is averaged over the same period as in (a–c). The reference arrows for the radial and vertical winds are 5 and 0.5 m·s^{-1}, respectively. (h) Same as in (g), but for the results of the CLM run during the same period as in (d–f).

implying that Nicole, examined in this study, is not an extraordinary case (not shown).

Long-term ocean observations have shown rapid warming (e.g., Yang et al., 2016) and significantly increased ocean eddy activity (e.g., Martínez-Moreno et al., 2021) in western boundary currents in recent years. It is anticipated that the recent trends will modulate the remote process discussed in this study and FK21. Therefore, future studies on statistical relationships between the recently observed changes in the warm currents, such as rapidly warming and increasing ocean eddy activities, and the recent TC activities in boreal fall are required in terms of the remote process proposed by this study and FK21.

AUTHOR CONTRIBUTIONS

KEITA FUJIWARA: Conceptualization; investigation; methodology; visualization; writing – original draft; writing – review and editing. **RYUICHI KAWAMURA:** Conceptualization; funding acquisition; project administration; resources; supervision; writing – review and editing.

ACKNOWLEDGEMENTS

The authors would like to thank Dr. Rhys Parfitt and three anonymous reviewers for their important comments and useful suggestions. We used the following publicly available data: HURDAT2 (available at https://www.nhc.noaa.gov/data/#hurdat), OISST V2.1 (available at https://www.ncei.noaa.gov/products/optimum-interpolation-sst), and NCEP GFS data (available at https://rda.ucar.edu/datasets/ds084.1/). In Figure 1, we used the Japanese 55-year Reanalysis (available at http://search.diasjp.net/ja/dataset/JRA55), J-OFURO3 (available at http://search.diasjp.net/en/dataset/JOFURO3_V1_1), and DUACS (available at https://cds.climate.copernicus.eu/cdsapp#!/dataset/satellite-sea-level-global?tab=overview). This research was supported by JSPS KAKENHI grants JP19H05696, JP20H00289, and JP20J11837.

ORCID

Keita Fujiwara https://orcid.org/0000-0002-4102-0943

REFERENCES

Deardorff, J.W. (1980) Stratocumulus-capped mixed layers derived from a three-dimensional model. *Boundary-Layer Meteorology*, 18, 495–527.

Ducet, N., Le Traon, P.-Y. & Reverdin, G. (2000) Global high-resolution mapping of ocean circulation from TOPEX/Poseidon and ERS-1 and-2. *Journal of Geophysical Research: Oceans*, 105, 19477–19498.

Fujiwara, K. & Kawamura, R. (2021) Active role of sea surface temperature changes over the Kuroshio in the development of distant tropical cyclones in boreal fall. *Journal of Geophysical Research: Atmospheres*, 126, JD035056. https://doi.org/10.1029/2021JD035056

Fujiwara, K., Kawamura, R., Hirata, H., Kawano, T., Kato, M. & Shinoda, T. (2017) A positive feedback process between tropical cyclone intensity and the moisture conveyor belt assessed with Lagrangian diagnostics. *Journal of Geophysical Research: Atmospheres*, 122, 12502–12521.

Fujiwara, K., Kawamura, R. & Kawano, T. (2020a) Remote thermodynamic impact of the Kuroshio current on a developing tropical cyclone over the western North Pacific in boreal fall. *Journal of Geophysical Research: Atmospheres*, 125, JD031356. https://doi.org/10.1029/2019JD031356

Fujiwara, K., Kawamura, R. & Kawano, T. (2020b) Suppression of tropical cyclone development in response to a remote increase in the latent heat flux over the Kuroshio: a case study for Typhoon Chaba in 2010. *Scientific Online Letters on the Atmosphere*, 16, 151–156.

Hegde, A.K., Kawamura, R. & Kawano, T. (2016) Evidence for the significant role of sea surface temperature distributions over remote tropical oceans in tropical cyclone intensity. *Climate Dynamics*, 47, 623–635.

Hong, X., Chang, S.W., Raman, S., Shay, L.K. & Hodur, R. (2000) The interaction between Hurricane Opal (1995) and a warm core ring in the Gulf of Mexico. *Monthly Weather Review*, 128, 1347–1365.

Huang, B., Liu, C., Banzon, V., Freeman, E., Graham, G., Hankins, B. et al. (2021) Improvements of the daily optimum interpolation sea surface temperature (DOISST) version 2.1. *Journal of Climate*, 34, 2923–2939.

Ikawa, M. & Saito, K. (1991) *Description of a nonhydrostatic model developed at the forecast research department of the MRI. Technical reports of the Meteorological Research Institute*. Japan: Meteorological Research Institute.

Jaimes, B., Shay, L.K. & Halliwell, G.R. (2011) The response of quasigeostrophic oceanic vortices to tropical cyclone forcing. *Journal of Physical Oceanography*, 41, 1965–1985.

Kobayashi, S., Ota, Y., Harada, Y., Ebita, A., Moriya, M., Onoda, H. et al. (2015) The JRA-55 reanalysis: general specifications and basic characteristics. *Journal of the Meteorological Society of Japan*, 93, 5–48.

Kondo, J. (1975) Air–sea bulk transfer coefficients in diabatic conditions. *Boundary-Layer Meteorology*, 9, 91–112.

Landsea, C.W. & Franklin, J.L. (2013) Atlantic hurricane database uncertainty and presentation of a new database format. *Monthly Weather Review*, 141, 3576–3592.

Li, D.Y. & Huang, C.Y. (2019) The influences of ocean on intensity of Typhoon Soudelor (2015) as revealed by coupled modeling. *Atmospheric Science Letters*, 20(1), e871.

Liang, J., Wu, L. & Gu, G. (2018) Rapid weakening of tropical cyclones in monsoon gyres over the tropical Western North Pacific. *Journal of Climate*, 31, 1015–1028.

Lin, I.-I., Wu, C.-C., Emanuel, K.A., Lee, I.-H., Wu, C.-R. & Pun, I.-F. (2005) The interaction of Supertyphoon Maemi (2003) with a warm ocean Eddy. *Monthly Weather Review*, 133, 2635–2649.

Lin, I.-I., Wu, C.-C., Pun, I.-F. & Ko, D.-S. (2008) Upper-ocean thermal structure and the Western North Pacific category 5 typhoons. Part I: ocean features and the category 5 typhoons' intensification. *Monthly Weather Review*, 136, 3288–3306.

Louis, J.F., Tiedtke, M. & Geleyn, J.F. (1981) A short history of the operational PBL parameterization at ECMWF. In Proceedings on ECMWF workshop on planetary boundary layer parameterization, Reading, United Kingdom, ECMWF, pp. 59–79. Available from: https://www.ecmwf.int/file/23088/download?token=g93a5QuY

Ma, Z. (2020) A study of the interaction between Typhoon Francisco (2013) and a cold-Core Eddy. Part I: rapid weakening. *Journal of the Atmospheric Science*, 77, 355–377.

Ma, Z., Fei, J., Liu, L., Huang, X. & Li, Y. (2017) An investigation of the influences of mesoscale ocean eddies on tropical cyclone intensities. *Monthly Weather Review*, 145(4), 1181–1201.

Martínez-Moreno, J., Hogg, A.M., England, M.H., Constantinou, N. C., Kiss, A.E. & Morrison, A.K. (2021) Global changes in oceanic mesoscale currents over the satellite altimetry record. *Nature Climate Change*, 11, 397–403.

Murakami, M. (1990) Numerical modeling of dynamical and microphysical evolution of an isolated convective cloud: the 19 July

1981 CCOPE cloud. *Journal of the Meteorological Society of Japan Series II*, 68, 107–128.

Murakami, M., Clark, T.L. & Hall, W.D. (1994) Numerical simulations of convective snow clouds over the sea of Japan: two-dimensional simulations of mixed layer development and convective snow cloud formation. *Journal of the Meteorological Society of Japan Series II*, 72, 43–62.

NCEP. (2015) NCEP GFS 0.25 degree global forecast grids historical archive. Available from: https://rda.ucar.edu/datasets/ds084.1/

Renault, L., McWilliams, J.C. & Masson, S. (2017) Satellite observations of imprint of oceanic current on wind stress by air–sea coupling. *Scientific Reports*, 7, 17747.

Shay, L.K. (2010) Air-sea interactions in tropical cyclones. In: Chan, J.C.L. & Kepert, J.D. (Eds.) *Global perspectives on tropical cyclones: from science to mitigation*. Singapore: World Scientific, pp. 93–131.

Shay, L.K., Goni, G.J. & Black, P.G. (2000) Effects of a warm oceanic feature on hurricane opal. *Monthly Weather Review*, 128, 1366–1383.

Sun, J., Wang, G., Xiong, X., Zhenli, H., Xiaomin, H., Zheng, L. et al. (2020) Impact of warm mesoscale eddy on tropical cyclone intensity. *Acta Oceanologica Sinica*, 39, 1–13.

Taburet, G., Sanchez-Roman, A., Ballarotta, M., Pujol, M.-I., Legeais, J.-F., Fournier, F. et al. (2019) DUACS DT2018: 25 years of reprocessed sea level altimetry products. *Ocean Science*, 15, 1207–1224.

Tomita, H., Hihara, T., Kako, S., Kubota, M. & Kutsuwada, K. (2019) An introduction to J-OFURO3, a third-generation Japanese ocean flux data set using remote-sensing observations. *Journal of Oceanography*, 75, 171–194.

Tomita, H., Kutsuwada, K., Kubota, M. & Hihara, T. (2021) Advances in the estimation of global surface net heat flux based on satellite observation: J-OFURO3 V1.1. *Frontiers in Marine Science*, 8, 612361.

Tsuboki, K. & Sakakibara, A. (2002) Large-scale parallel computing of cloud resolving storm simulator. In: *High performance computing*. New York, NY: Springer, pp. 243–259. https://doi.org/10.1007/3-540-47847-7_21

Wada, A., Tomita, H. & Kako, S. (2020) Comparison of the third-generation Japanese ocean flux data set J-OFURO3 with numerical simulations of Typhoon Dujuan (2015) traveling south of Okinawa. *Journal of Oceanography*, 76, 419–437.

Wu, C.-C., Lee, C.-Y. & Lin, I.-I. (2007) The effect of the ocean Eddy on tropical cyclone intensity. *Journal of the Atmospheric Science*, 64, 3562–3578.

Yang, H., Lohmann, G., Wei, W., Dima, M., Ionita, M. & Liu, J. (2016) Intensification and poleward shift of subtropical western boundary currents in a warming climate. *Journal of Geophysical Research: Oceans*, 121, 4928–4945.

SUPPORTING INFORMATION

Additional supporting information can be found online in the Supporting Information section at the end of this article.

How to cite this article: Fujiwara, K., & Kawamura, R. (2023). Intensification of a distant hurricane by warm-core eddies in the Gulf Stream in boreal fall. *Atmospheric Science Letters*, *24*(3), e1141. https://doi.org/10.1002/asl.1141